第 50 卷 第 14 期/2023 年 7 月/中国激光 研究论文

中国激光

大角度双波段探测成像分光器件的研制

付秀华[1,2]，刘瑞奇[1*]，朱忠尧[3]，韩克旭[1]，王奔[2]，刘俊岐[1]，刘海成[1]

[1]长春理工大学光电工程学院，吉林 长春 130022；

[2]长春理工大学中山研究院，广东 中山 528436；

[3]北京空间机电研究所，北京 100094

摘要 在微光夜视与红外成像融合的光学系统中，光通过55°放置的分光镜分成两束光，其中反射光被微光探测器接收进行微光夜视成像，透射光被红外探测器接收进行红外成像，通过图像融合技术来提高系统的成像分辨率。针对分光镜的参数要求，笔者选用Ge、ZnS和YbF_3作为沉积材料，采用离子源辅助沉积技术在多光谱ZnS基底上制备了0.6～0.9 μm波段高反、3.7～4.8 μm波段高透的分光膜。通过对膜系结构的优化以及沉积工艺参数的调整，解决了膜层牢固度和面形精度等问题，实现了0.6～0.9 μm波段反射率为90.77%、3.7～4.8 μm波段透射率为91.15%的分光指标。附着力测试、摩擦力测试、高低温测试、恒温恒湿测试结果显示所制备的双面膜可以满足使用要求，但该膜的短波反射率和长波透过率仍有一定的提升空间。

关键词 光学器件；分光镜；微光夜视；中波红外成像；面形精度

中图分类号 O484 **文献标志码** A **DOI:** 10.3788/CJL221490

1 引 言

随着我国军用光学技术的不断更新迭代，单一波段光谱已远远不能满足特定场景的使用需求，需要根据不同波段成像质量的优劣选择多波段成像，从成像技术上不断提高传感器的质量。因此，图像融合技术越来越受到关注，并对光学系统中的光学元件提出了更高要求[1-2]。

目前，多光谱融合技术已被广泛应用于军事作战、医学影像分析等领域[3-4]。2014—2018年，我国科研人员[5-8]研究了0.5～9.3 μm波段范围内的双波段或三波段增透膜系，其在该波段的平均透过率能达到95%以上。2018年，Fleming等[9]采用脉冲磁控溅射的方式制备了4.2 μm带通滤光膜。2021年，Guo等[10]研制了0°入射时，在0.3～0.9 μm波段的平均透射率低于1%且在3.7～4.8 μm波段的平均透射率超过92%的滤光片。

综上所述，国内外在红外图像融合领域进行了广泛研究，但目前针对可见/近红外、中红外双波段大角度分光镜的研究还鲜有报道，该研究对于双波段红外探测成像技术具有重要的参考意义。

2 材料选取

辐射传输常用的红外基底有Ge、Si、ZnS、ZnSe、蓝宝石(Al_2O_3)等。分析后认为ZnS更适合作为基底。相较于普通的ZnS，多光谱ZnS具有透射波段更宽、吸收更小、透过率更高的特点[11]，如图1(a)所示。红外波段常见的镀膜材料的可选择性较小，大部分在可见波段有吸收。能满足覆盖可见到中红外波段的低折射率薄膜材料主要有ThF_4、YbF_3和YF_3，其中：ThF_4有放射性；YbF_3和YF_3的光学性质相似，但对于采用同种工艺镀制的相同厚度的YbF_3和YF_3来说，后者的应力更大，更容易出现脱膜裂膜现象。因而，本次实验选用YbF_3作为低折射率材料。采用Macleod对YbF_3单层膜进行拟合得到了其折射率曲线，如图1(b)所示。

考虑到薄膜的物理特性以及基底本身就是ZnS，分光面上的高折射率材料选择ZnS。Ge的折射率高，且与ZnS匹配度高，故增透膜中的高折射率材料选择Ge。采用Macleod对单层膜进行拟合得到的薄膜的折射率如图2所示。

收稿日期：2022-12-05；**修回日期**：2022-12-07；**录用日期**：2023-02-08；**网络首发日期**：2023-03-18

基金项目：2022年度中山市第二批社会公益与基础研究项目(2022B2005)、"十三五"共用技术预研基金(41423060202)、长春市激光制造与检测装备科技创新中心资助项目(长科技合(2014219)号)

通信作者：*1265567047@qq.com

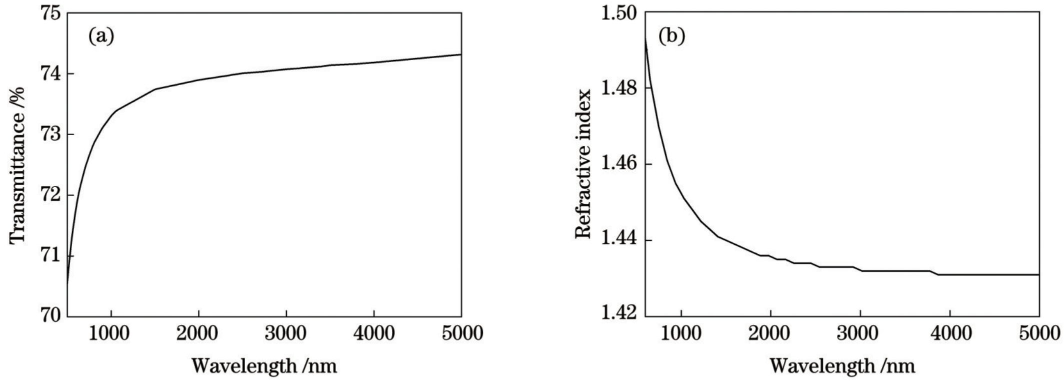

图 1　材料性能。(a) ZnS 基底的透射曲线；(b) YbF_3 的折射率

Fig. 1　Materials performances. (a) Transmittance curve of ZnS substrate; (b) refractive index of YbF_3

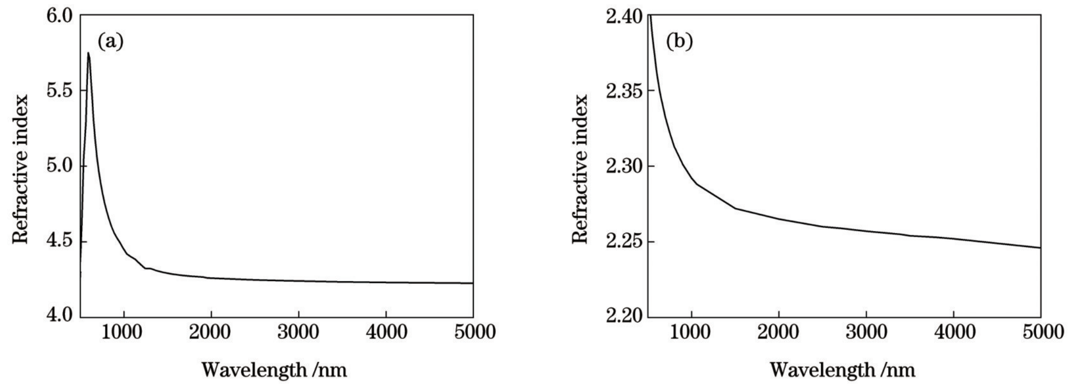

图 2　薄膜的折射率。(a) Ge；(b) ZnS

Fig. 2　Refractive index of two films. (a) Ge; (b) ZnS

3　膜系设计

分光镜是探测系统中的关键部件，其薄膜的主要技术参数如表 1 所示。

对表 1 所示技术指标进行分析可知，该膜系短波高反长波高透，类似于一个基础结构为$(0.5HL0.5H)^s$的长波通。对称膜堆用矩阵方法进行计算，公式[12]为

$$\boldsymbol{M}_{\mathrm{H}}=\begin{bmatrix}\cos\delta_{\mathrm{H}} & \dfrac{\mathrm{i}\sin\delta_{\mathrm{H}}}{\eta_{\mathrm{H}}}\\ \mathrm{i}n_{\mathrm{H}}\sin\delta_{\mathrm{H}} & \cos\delta_{\mathrm{H}}\end{bmatrix},\tag{1}$$

$$\boldsymbol{M}_{\mathrm{L}}=\begin{bmatrix}\cos\delta_{\mathrm{L}} & \mathrm{i}\sin\delta_{\mathrm{L}}\\ \mathrm{i}n_{\mathrm{L}}\delta\sin\delta_{\mathrm{L}} & \cos\delta_{\mathrm{L}}\end{bmatrix},\tag{2}$$

$$\boldsymbol{M}=\boldsymbol{M}_{\mathrm{H}}\boldsymbol{M}_{\mathrm{L}}\boldsymbol{M}_{\mathrm{H}}\cdots\boldsymbol{M}_{\mathrm{H}}\boldsymbol{M}_{\mathrm{L}}\boldsymbol{M}_{\mathrm{H}}=\begin{bmatrix}m_{11} & m_{12}\\ m_{21} & m_{22}\end{bmatrix},\tag{3}$$

表 1　薄膜的技术指标

Table 1　Technical specifications of film

Parameter	Indicator
Spectrum range /μm	0.6–0.9, 3.7–4.8
Reflectivity R	>90%
Transmittance T	>90%
Incident angle /(°)	55±3
Peak-valley (PV) value of spectral surface /λ	≤0.2
PV value of antireflection surface /λ	≤0.4

式中：δ_{H}、δ_{L}分别表示高折射率材料和低折射率材料的相位差；n_{H}、n_{L}分别表示高低折射率材料的折射率；η表示材料的折射率(包括斜入射情况)。通过矩阵运算可求得

$$m_{11}=m_{22}=\cos(2\delta_{\mathrm{H}})\cos\delta_{\mathrm{L}}-\frac{1}{2}\left(\frac{\eta_{\mathrm{L}}}{\eta_{\mathrm{H}}}+\frac{\eta_{\mathrm{H}}}{\eta_{\mathrm{L}}}\right)\sin(2\delta_{\mathrm{H}})\sin\delta_{\mathrm{L}},\tag{4}$$

$$m_{12}=\frac{\mathrm{i}}{\eta_{\mathrm{H}}}\left[\sin(2\delta_{\mathrm{H}})\cos\delta_{\mathrm{L}}+\frac{1}{2}\left(\frac{\eta_{\mathrm{H}}}{\eta_{\mathrm{L}}}+\frac{\eta_{\mathrm{L}}}{\eta_{\mathrm{H}}}\right)\cos(2\delta_{\mathrm{H}})\sin\delta_{\mathrm{L}}+\frac{1}{2}\left(\frac{\eta_{\mathrm{H}}}{\eta_{\mathrm{L}}}+\frac{\eta_{\mathrm{L}}}{\eta_{\mathrm{H}}}\right)\sin\delta_{\mathrm{L}}\right],\tag{5}$$

$$m_{21}=\frac{\mathrm{i}}{\eta_{\mathrm{H}}}\left[\sin(2\delta_{\mathrm{H}})\cos\delta_{\mathrm{L}}+\frac{1}{2}\left(\frac{\eta_{\mathrm{H}}}{\eta_{\mathrm{L}}}+\frac{\eta_{\mathrm{L}}}{\eta_{\mathrm{H}}}\right)\cos(2\delta_{\mathrm{H}})\sin\delta_{\mathrm{L}}-\frac{1}{2}\left(\frac{\eta_{\mathrm{H}}}{\eta_{\mathrm{L}}}-\frac{\eta_{\mathrm{L}}}{\eta_{\mathrm{H}}}\right)\sin\delta_{\mathrm{L}}\right]。\tag{6}$$

当$|m_{11}|>1$时，等效导纳为虚数，即当膜层足够多时该波段为截止带；当$|m_{11}|<1$时，等效导纳为实数，该波段为透射带；当$|m_{11}|=1$时，表示该波段是透射带向截止带过渡的波段，如图 3 所示。

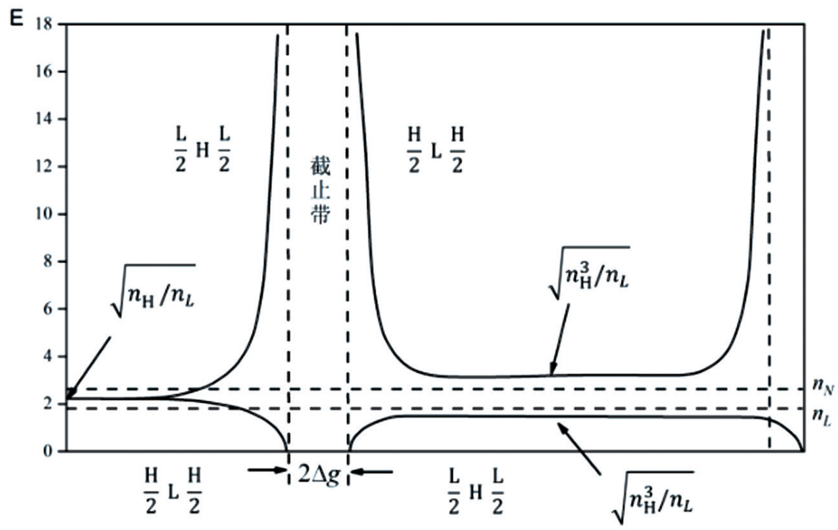

图 3　对称周期膜系在垂直入射时的等效折射率 E[13]

Fig. 3　Equivalent refractive index E of symmetrical periodic film systems under vertical incidence[13]

长波通光谱曲线的反射带波数宽度 Δg 为

$$\Delta g=\frac{2}{\pi}\arcsin\left(\frac{n_H-n_L}{n_H+n_L}\right), \tag{7}$$

波长宽度为

$$\Delta\lambda=2\Delta g\lambda_0, \tag{8}$$

式中：n_H、n_L 表示 0°入射时高低折射率材料的折射率；λ_0 表示参考波长。

当高折射率材料（H）为 ZnS，低折射率材料（L）为 YbF_3 时，长波通截止带波长宽度约为 100 nm，考虑 55°入射，需要 4 个膜堆叠加，故膜系基础结构设计为 Sub|1.4(0.5HL0.5H)^{10} 1.26(0.5HL0.5H)^{10} 1.14(0.5HL0.5H)^{10} (0.5HL0.5H)^{10} |Air，其中 Sub 表示多光谱 ZnS 基板，Air 表示空气。采用膜系设计软件进行优化，得到膜系结构为 Sub|0.494H1.0149L2.38H0.563L…0.467L0.77H2.8L0.482H|Air，其理论光谱曲线如图 4(a)所示，其总层数为 80 层，总厚度约为 10 μm。

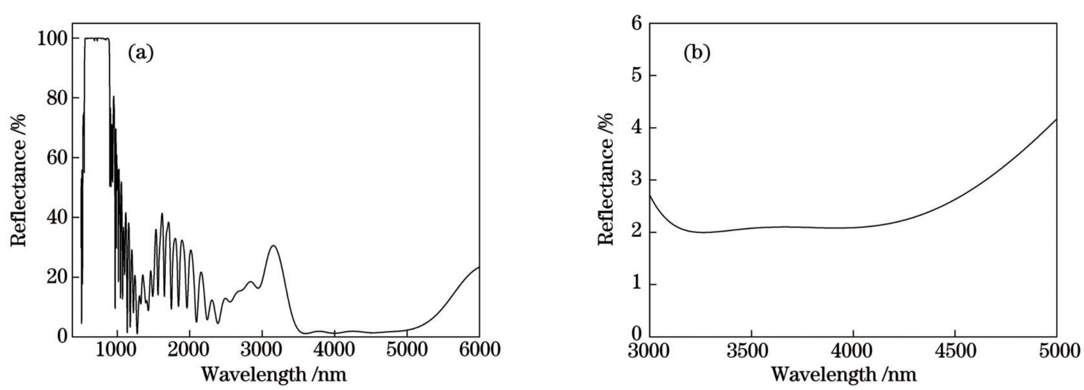

图 4　55°入射时分光面和增透面的理论光谱。(a)分光面；(b)增透面

Fig. 4　Theoretical spectra of spectral surface and antireflection surface with 55° incidence. (a) Spectral surface; (b) antireflection surface

基板的另一面需要设计 3.7～4.8 μm 增透膜。依据增透膜设计理论，选择基础膜系 Sub|(HL)^{2}M|Air 进行优化，得到膜系结构为 Sub|0.27H2.04L0.147H0.452L2.188M|Air，其中 H 表示高折射率材料 Ge，L 表示中折射率材料 ZnS，M 表示低折射率材 YbF_3。经过实验验证，将 YbF_3 作为最外层会出现划痕、龟裂和脱膜等问题，因此，在最外层增加 ZnS 层，这样既能起到保护作用还能降低 YbF_3 的厚度。最终的设计膜系为 Sub|0.414H1.742L0.508H 1.666M 0.361L|Air，设计光谱曲线如图 4(b)所示。

双面设计的理论光谱曲线如图 5 所示，其中 0.6～0.9 μm 波段的平均反射率为 98.8%，3.7～4.8 μm 波段

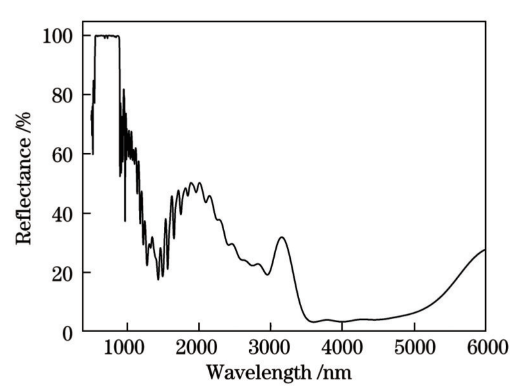

图 5　双面设计的理论光谱

Fig. 5　Theoretical spectrum with double-sided design

的平均透射率为96.3%。

4　镀膜实验

镀膜实验在OTFC-1300蒸发镀膜机上完成。该设备配备霍尔离子源和XTC/3晶体膜厚控制系统，Ge薄膜采用电子束蒸发制备，ZnS、YbF_3薄膜采用电阻蒸发制备。Ge、ZnS、YbF_3薄膜的沉积工艺参数如表2所示。

表2　Ge、ZnS、YbF_3薄膜的沉积工艺参数

Table 2　Deposition parameters of Ge, ZnS and YbF_3 films

Film layer	Deposition rate/ (nm·s^{-1})	Chamber pressure/(10^{-4} Pa)	Rotation rate/ (rad·min^{-1})	Deposition temperature /℃
Ge	0.5	4	25	160
ZnS	2	4	25	160
YbF_3	0.4	4	25	160

镀膜前恒温1 h，采用离子源清洗基板15 min。为保证薄膜材料与基板的结合度，同时保证二者应力匹配，全程使用离子源辅助沉积。ZnS和YbF_3在不同蒸发条件下的应力值不同。与电子束加热蒸发相比，电阻蒸发制备的薄膜的应力较小，折射率更低，因此采用电阻蒸发的方式沉积。真空退火工艺对应力、膜层牢固度、膜层表面形貌均有很大影响。镀膜结束后在200 ℃恒温2 h，随后自然降温至90 ℃，放气[14-16]。离子源沉积工艺参数如表3所示

表3　离子源沉积工艺参数

Table 3　Process parameters of ion source deposition

Material	Anodic voltage /V	Ion beam current /mA	Flow of argon gas /(mL·min^{-1})
Ge	150	1	20
ZnS	150	1	20
YbF_3	200	5	20
Cleaning	180	3	25

5　测试与分析

5.1　应力检测与分析

蒸发镀制的ZnS薄膜中的应力通常为压应力，而蒸发镀制的YbF_3薄膜中的应力通常为张应力。依据控制变量的方法，通过改变沉积工艺来调整相应厚度ZnS、YbF_3单层膜的应力值。由于膜系是高低折射率材料交替沉积而成的，张应力和压应力可以相互抵消，因此相应厚度的高低折射率材料的单层膜的应力值越接近，基板的形变量就越小。根据测得的应力分析膜系结构，在设计上考虑双面薄膜应力能够相互抵消或趋于更小。应力计算需要借助Stoney公式，其表达式[17]为

$$R=\frac{1}{2}\left(\frac{r^2}{h}+h\right)\approx\frac{r^2}{2h},\tag{9}$$

$$\sigma=\frac{E_z d_z^2}{6\left(1-v^2\right)d_f}\left(\frac{1}{R_f}-\frac{1}{R_0}\right),\tag{10}$$

式中：R为曲率半径；σ为薄膜的应力值；h为干涉仪测得的power值；E_z为基板的杨氏模量；d_z为基板的厚度；v为基板的泊松比；d_f为薄膜厚度；R_0为镀膜前基板的曲率半径；R_f为镀膜后基板的曲率半径；r为基板半径。

利用激光干涉仪测量两片Ø30 mm圆形硫化锌基底沉积单层薄膜前后的面形，测试结果和计算结果如表4所示，其中λ=632.8 nm。

表4　单层膜的应力变化表

Table 4　Stress variation table of single-layer membrane

Film layer	Film thickness /nm	Power /λ		Stress /MPa	
		Before evaporation	After evaporation	Before process adjustment	After process adjustment
ZnS	4261.6	0.138	−1.24	180	208
YbF_3	6127.4	0.172	1.47	276	222

分析工艺调整前的参数可知，单层ZnS的应力值与单层YbF_3的应力值不匹配。调整ZnS和YbF_3的沉积速率以及离子源辅助工艺，将ZnS的沉积速率由2 nm/s调整为1.5 nm/s，YbF_3离子源辅助沉积参数由200 V、5 A调整为220 V、5 A。调整工艺参数后，单层ZnS与单层YbF_3的应力值接近。

基底镀膜前，测得表面面形的峰谷值（PV值）为0.136λ；长波通镀制结束后，测得PV值为0.63λ。镀膜前后的面形差异较大，因此需要对增透面进行应力补偿。计算得分光膜系的应力为326 MPa，增透膜系的应力为162 MPa，随后进行双面膜镀制实验。测得双面膜分光面的PV值为0.182λ，增透面的PV值为

0.228λ，如图 6 所示。可见，工艺调整后达到了降低薄膜应力、优化表面面形的目的。

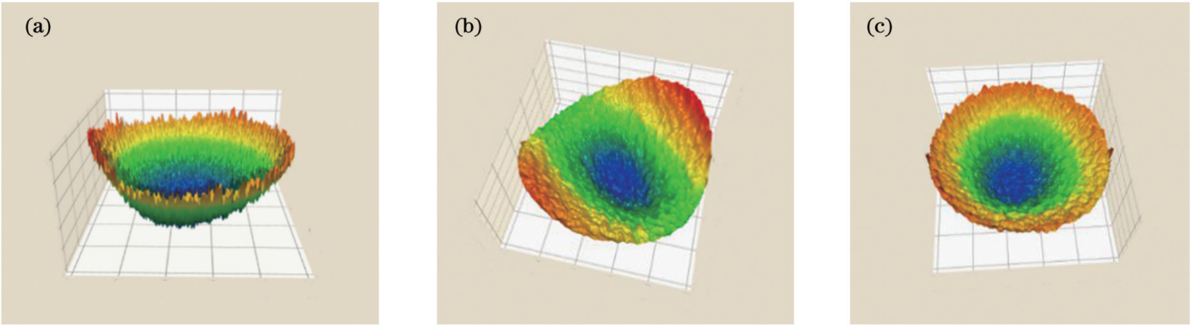

图 6 基板、分光面和增透面的面形。(a)基板；(b)分光面；(c)增透面

Fig. 6 Surface shape of substrate, spectral surface and antireflection surface. (a) Substrate; (b) spectral surface; (c) antireflection surface

5.2 光谱检测结果分析

使用 Cary 7000 分光光度计与 Spectrum Two 傅里叶光谱仪分别对可见/近红外和中红外光谱进行测试。依据所获得的薄膜材料的折射率与消光系数设计分光膜的光谱，对设计光谱与实际光谱进行比较后发现实际光谱整体右移，长波透过率偏低，如图 7 所示。

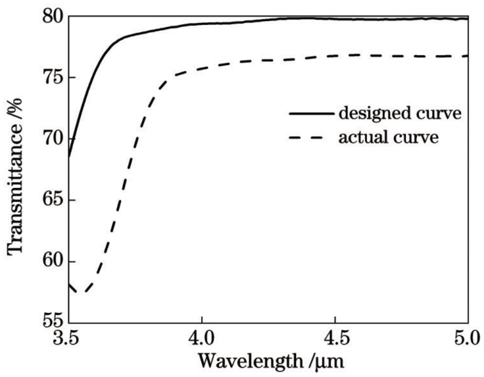

图 7 理论设计光谱与实际光谱的对比

Fig. 7 Comparison of theoretically designed spectrum and actual spectrum

将光谱数据导入 Macleod 进行拟合后发现，ZnS 的实际厚度是设计厚度的 1.08 倍，YbF_3的实际厚度是设计厚度的 95%。调整膜层厚度比例后沉积双面膜，其分光面透射光谱如图 8 所示，光谱整体上与设计光谱拟合得较好，无明显偏差。在单面镀膜条件下，3.7～4.8 μm 波段的理论平均透过率为 79.5%，实测平均透过率为 77%。对实测光谱进行拟合，结果显示光谱性能变差不是由膜层厚度失配导致的。分析后发现，在调节应力匹配过程中增加离子源辅助沉积导致 ZnS 与 YbF_3膜层的吸收增大，但仍满足技术指标。

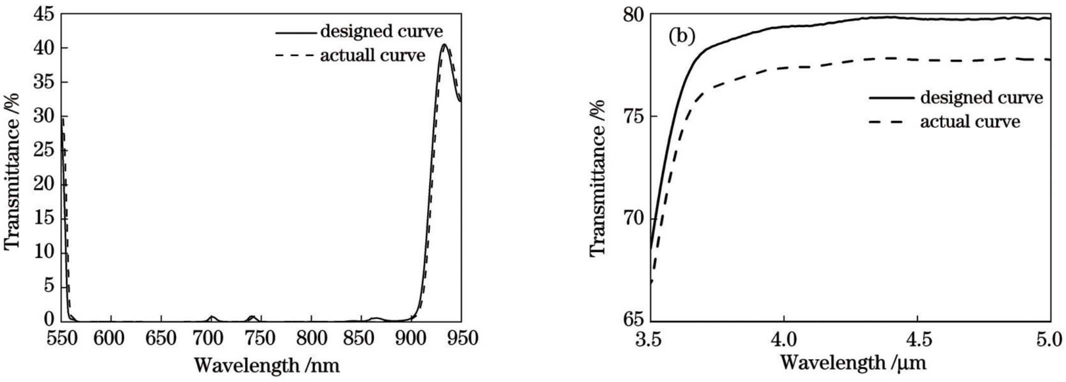

图 8 分光面设计光谱与实际光谱的对比。(a)可见/近红外光谱；(b)中红外光谱

Fig. 8 Designed and actual spectra comparison for spectral surface. (a) Visible/near-infrared spectra; (b) mid-infrared spectra

在多光谱 ZnS 基底上完成双面膜的制备后进行光谱测试。当入射角为 55°时，双面膜在 0.6～0.9 μm 波段的反射率为 90.77%，在 3.7～4.8 μm 波段的透过率为 91.15%，如图 9 所示，可以满足设计要求。样片实物图如图 10 所示。

5.3 根据使用要求对样品进行环境测试

附着力测试：将 3 mm 宽的拉力胶带粘贴在膜层表面，快速垂直将胶带撕下，重复 5 次，无脱膜现象发生。

摩擦力测试：用无尘布紧裹住橡皮擦，加 1 kg 砝码，在膜层表面沿同一轨迹重复摩擦 25 次，无擦痕出现。

高低温测试：将样片放入冷热对冲箱内，先在低温 −62 ℃±2 ℃下保持 2 h，而后在高温 85 ℃±2 ℃下

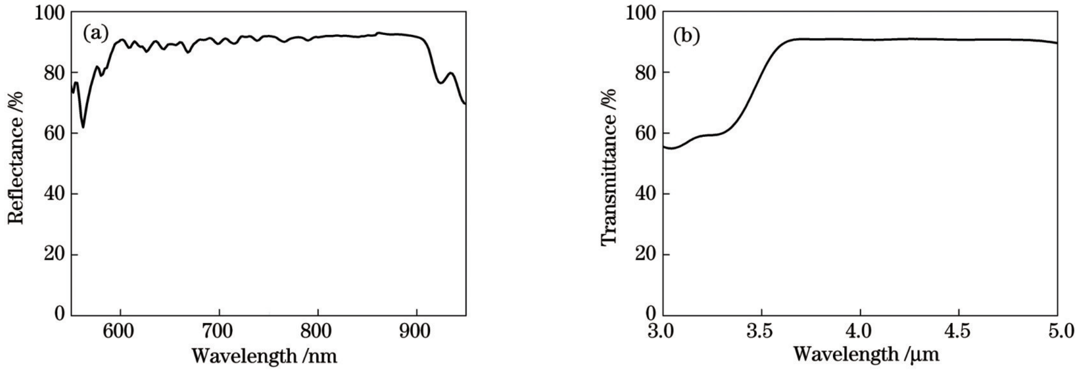

图 9 双面膜样品的反射率和透射率。(a)0.6～0.9 μm 波段的反射率;(b)3.7～4.8 μm 波段的透过率

Fig. 9 Reflectivity and transmittance of double-sided film samples. (a) Reflectivity in band 0.6–0.9 μm; (b) transmittance in band 3.7–4.8 μm

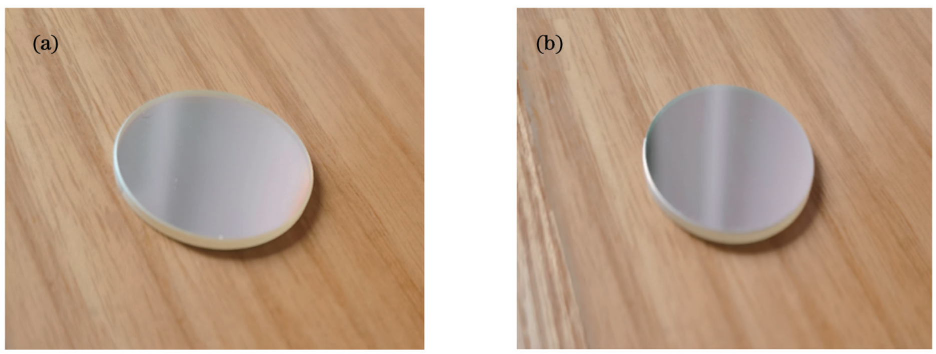

图 10 样片实物图。(a)分光面;(b)增透面

Fig. 10 Sample physical photos. (a) Spectral surface; (b) antireflection surface

保持 2 h,进行 4 个程式测试后观察,膜层没有明显变化。

恒温恒湿测试:将样片放入湿热箱内,温度为 45 ℃±2 ℃,相对湿度为 95%～100%,放置 24 h 后取出观察,膜层没有明显变化。

6 结 论

采用控制变量法对温度、沉积方法、离子源辅助沉积参数进行调整,利用 Stoney 公式计算膜层应力,进而对特定厚度的单层膜 ZnS、YbF_3中的应力进行调整,使单层膜 ZnS、YbF_3的应力相匹配。利用增透面的应力补偿分光面的应力,分光面的面形精度(PV 值)从 0.63λ 降到 0.182λ,解决了分光镜表面面形差的问题。通过对薄膜沉积结果进行逆向反演分析,调整膜层厚度,提升了薄膜在 55°入射时的反射率和透射率,其在 0.6～0.9 μm 波段的平均反射率为 90.77%,在 3.7～4.8 μm 波段的平均透过率为 91.15%。

制备的薄膜基本满足系统元件的使用需求,但短波反射率和长波透过率仍有提升空间,在后续研究中将以提高光谱性能为主要工作。

参 考 文 献

[1] 胡海力, 贺磊, 张勇, 等. 低照度背景下弱小目标的成像实验研究[J]. 红外与激光工程, 2020, 49(9): 20190569.
Hu H L, He L, Zhang Y, et al. Imaging experiments for weak small target in low-light-level background[J]. Infrared and Laser Engineering, 2020, 49(9): 20190569.

[2] 黄煜东. 真实场景的红外与微光图像融合方法研究[D]. 长沙: 国防科技大学, 2018.
Huang Y D. Fusion of infrared and low-level light images in realistic scene[D]. Changsha: National University of Defense Technology, 2018.

[3] 陶媛媛. 红外与微光融合夜视系统性能评价[D]. 南京: 南京理工大学, 2015.
Tao Y Y. Performance evaluation of infrared and low light level fusion night vision system[D]. Nanjing: Nanjing University of Science and Technology, 2015.

[4] 谢一博, 徐乃涛, 周顺, 等. 分布式红外阵列相机的超分辨图像重建研究[J]. 激光与光电子学进展, 2022, 59(16): 1611004.
Xie Y B, Xu N T, Zhou S, et al. Super-resolution image reconstruction of distributed infrared array camera[J]. Laser & Optoelectronics Progress, 2022, 59(16): 1611004.

[5] 王彤彤. 基于氧化物的 0.8～1.7 μm 和 3.7～4.8 μm 硬质宽带红外增透膜研制[J]. 中国光学, 2014, 7(5): 816-822.
Wang T T. Fabrication of hard infrared anti-reflection coating with broadband in the wavelength of 0.8–1.7 μm and 3.7–4.8 μm based on oxide material[J]. Chinese Optics, 2014, 7(5): 816-822.

[6] 张天行, 李钱陶, 何光宗, 等. 硫化锌基底硬质红外保护薄膜技术研究[J]. 光学与光电技术, 2015, 13(3): 50-53.
Zhang T X, Li Q T, He G Z, et al. Research of hard protective infrared coatings on ZnS substrate[J]. Optics & Optoelectronic Technology, 2015, 13(3): 50-53.

[7] 米高园, 张建付, 韩俊, 等. 电视、激光、中波红外多波段增透膜研究[J]. 激光与红外, 2016, 46(5): 593-596.
Mi G Y, Zhang J F, Han J, et al. Research on antireflection coating for TV, laser, mid-infrared wavebands[J]. Laser & Infrared, 2016, 46(5): 593-596.

[8] 姜洪妍 . 短中波红外成像系统光学薄膜的研制[D]. 长春: 长春理工大学, 2018.
Jiang H Y. Development of short and medium wave infrared imaging system optical coating[D]. Changchun: Changchun University of Science and Technology, 2018.

[9] Fleming L, Gibson D, Song S G, et al. Reducing N_2O induced cross-talk in a NDIR CO_2 gas sensor for breath analysis using multilayer thin film optical interference coatings[J]. Surface and Coatings Technology, 2018, 336: 9-16.

[10] Guo M, Yi K, Cui X Q, et al. Design and preparation of UV-visible-shortwave near infrared cut-off and mid-infrared antireflection coating[J]. Optik, 2021, 227: 165470.

[11] 邢政, 付秀华, 傅晶晶, 等 . 650 nm 反射 10.6 μm 透射的薄膜干涉滤光片[J]. 激光与红外, 2008, 38(5): 482-484.
Xing Z, Fu X H, Fu J J, et al. Interference filter of reflectance in 650 nm and transmittance in 10.6 μm[J]. Laser & Infrared, 2008, 38(5): 482-484.

[12] 赵兴梅 . 长波通滤光片的研究[D]. 长春: 长春理工大学, 2004.
Zhao X M. Research of long-wavelength pass filter[D]. Changchun: Changchun University of Science and Technology, 2004.

[13] 唐晋发, 顾培夫, 刘旭 . 现代光学薄膜技术[M]. 杭州: 浙江大学出版社, 2006.
Tang J F, Gu P F, Liu X. Modern optical thin film technology [M]. Hangzhou: Zhejiang University Press, 2006.

[14] 冯毅东, 于天燕, 刘定权 . 沉积工艺对 YbF_3 薄膜可靠性的影响[J]. 光学学报, 2018, 38(7): 0731002.
Feng Y D, Yu T Y, Liu D Q. Influence of deposition process on reliability of YbF_3 thin films[J]. Acta Optica Sinica, 2018, 38(7): 0731002.

[15] 秦杨, 张荣福 . 不同温度制备氟化镱薄膜的工艺研究[J]. 光学仪器, 2018, 40(3): 90-94.
Qin Y, Zhang R F. Investigation on the preparation of YbF_3 films at different temperatures[J]. Optical Instruments, 2018, 40(3): 90-94.

[16] 陈焘, 罗崇泰, 王多书, 等 . 离子束辅助沉积和真空退火对硫化锌薄膜应力的影响[J]. 真空科学与技术学报, 2009, 29(S1): 55-58.
Chen T, Luo C T, Wang D S, et al. Influence of ion beam assistance deposition and annealing on stress in ZnS films[J]. Chinese Journal of Vacuum Science and Technology, 2009, 29 (S1): 55-58.

[17] 朱京涛, 郭胜, 赵娇玲, 等 . 脉冲直流溅射 Zr 薄膜的微结构和应力研究[J]. 光学学报, 2021, 41(18): 1831001.
Zhu J T, Guo S, Zhao J L, et al. Microstructure and stress of Zr thin film deposited by pulsed DC sputtering[J]. Acta Optica Sinica, 2021, 41(18): 1831001.

Fabrication of Large-Angle Dual-Band Detection Imaging Splitter

Fu Xiuhua[1,2], Liu Ruiqi[1*], Zhu Zhongyao[3], Han Kexu[1], Wang Ben[2], Liu Junqi[1], Liu Haicheng[1]

[1]*School of Opto-Electronic Engineering, Changchun University of Science and Technology, Changchun* 130022, *Jilin, China*;
[2]*Zhongshan Research Institute, Changchun University of Science and Technology, Zhongshan* 528436, *Guangdong, China*;
[3]*Beijing Institute of Space Mechatronics, Beijing* 100094, *China*

Abstract

Objective There are significant differences in the actual optical characteristics of specific targets in different spectral bands. Thus, the two imaging systems shared an aperture for detection and identification. The internal light was separately imaged after passing through an optical device that separated the visible near-infrared and infrared light. In this way, the light from the two bands could be used to synchronously detect and image the target, allowing it to track the target more effectively. Thus, it could meet the all-day, wide-range, and high-resolution detection requirements. There have been few research reports on visible near-infrared and mid-infrared dual-band large-angle spectroscopy. Therefore, this research has an important reference value for dual-band infrared detection and imaging technology.

Methods The width and reflectance of the cut-off band at large angles were studied using the evaporation coating method. After practical calculation, it was concluded that at least four groups of film stacks should be used as the initial film system. A spectral curve that met the requirements could be obtained based on this optimization of the initial film system. The stress of ZnS film is generally compressive, while the stress of YbF_3 film is generally tensile. The control variable method was used to optimize the deposition process and adjust the corresponding thickness to change the stress of the ZnS and YbF_3 single-layer films. Because the film system was formed by depositing alternate layers of high and low refractive index materials, the tensile stress and compressive stress could offset each other. Therefore, the deformation of the substrate was smaller when the single-layer stresses of the high and low refractive index materials with corresponding thicknesses were closer. The film system structure was analyzed based on the measured stress results, which showed that the two sides of the film could offset each other and tended to be smaller in the design.

Results and Discussions Based on a study of the characteristics of the high and low refractive index materials, the deposition process parameters of the film material (Table 2) were selected as the auxiliary parameters of the ion source (Table 3). Before coating, a constant temperature was 1 h. Thereafter, the ion source was used to clean the substrate for 15 min. A constant temperature of 200 ℃ was maintained for 2 h after coating, then the temperature was naturally cool to 90 ℃ for venting. The stress changes before and after coating are listed in Table 4. It can be seen from the analysis of the parameters before and after the process adjustment that the stress of the single-layer ZnS did not match that of the single-layer YbF_3. The ZnS and YbF_3 deposition rates and auxiliary process parameters of the ion source were adjusted. The ZnS deposition rate was adjusted from 2 nm/s to 1.5 nm/s, and the deposition parameters of the YbF_3 ion source was adjusted from 200 V and 5 A to 220 V and 5 A. After adjusting the process parameters, the stress of the single-layer ZnS was close to that of the single-layer YbF_3 (Table 4). The antireflective film coated on the reverse side presented a tensile stress state, which could compensate for the stress on the spectral surface. The antireflective film coated on the reverse side met the requirements (Fig. 6). The spectrum of the deposited film was obtained and analyzed (Fig. 7), and the spectral data were imported into the film system design software for fitting. It was found that the actual thickness of the ZnS was 1.08 times the design thickness, and the actual thickness of the YbF_3 was 0.95 times the design thickness. After adjusting the film thickness ratio, the transmission spectrum curve of the spectral surface after deposition (Fig. 8) showed that the overall spectrum was well fitted with the design without obvious deviation (transmittance of 3.7–4.8 μm under the condition of the single-sided coating). The theoretical average transmittance in the band of 3.7–4.8 nm was 79.5%, and the average measured transmittance was 77%. The measured spectrum was fitted, and the fitting results showed that the spectral performance was not caused by the mismatch of the film thickness. After analysis, it was found that the addition of ion source-assisted deposition in the adjustment of the stress matching resulted in an increase in the absorption of the ZnS and YbF_3 films but still met the technical specifications.

Conclusions In this study, the temperature, deposition method, and ion source parameters were adjusted using the control variable method. The film stress was calculated using the Stoney formula. Then, the stresses of specific-thickness single-layer ZnS and YbF_3 were adjusted to make these stresses match. When the stress of the antiantireflection surface was used to compensate for the stress of the spectral surface, the surface accuracy (PV value) of the spectral surface decreased from 0.63λ to 0.182λ. Then, the problem of the poor surface shape of the spectroscope could be solved. Based on a reverse analysis of the film deposition results, the film thickness was adjusted to improve the reflectivity and transmittance at an incidence of 55°. In the 0.6–0.9 μm wave band, the average reflectivity was 90.77%. In the 3.7 – 4.8 μm wave band, the average transmittance was 91.15%. The prepared film basically met the use requirements of the system components.

Key words optical devices; spectroscope; low light level night vision; medium wave infrared imaging; surface flatness